





Structural relaxation dynamics of colloidal nanotrimerJustinas Šlepavičius ¹, Carlos Avendaño ¹, Breannán Ó. Conchúir ^{1,2} and Alessandro Patti ^{1,3,*}¹*Department of Chemical Engineering, The University of Manchester, Manchester M13 9PL, United Kingdom*²*IBM Research Europe, The Hartree Centre STFC Laboratory Sci-Tech Daresbury Warrington, Warrington WA4 4AD, United Kingdom*³*Department of Applied Physics, University of Granada, Fuente Nueva s/n, 18071 Granada, Spain*

(Received 13 April 2022; accepted 29 June 2022; published 15 July 2022)

By Molecular Dynamics simulation, we investigate the dynamics of isotropic fluids of colloidal nanotrimers whose interactions are described by varying the strength of attractive and repulsive terms of the Mie potential. To provide a consistent comparison between the systems described by different force fields, we determine the phase diagram and critical points of each system, characterize the morphology of high-density liquid phases at the same reduced temperature and density, and finally investigate their long-time relaxation dynamics. In particular, we detect an especially complex dynamics that reveals the existence of slow and fast nanotrimers and the resulting occurrence of non-Gaussianity, which develops at intermediate timescales. Deviations from Gaussianity are temporary and vanish within the timescales of the system's density fluctuations decay, when a Fickian-like diffusion regime is eventually observed.

DOI: [10.1103/PhysRevE.106.014604](https://doi.org/10.1103/PhysRevE.106.014604)**I. INTRODUCTION**

Colloidal sols are two-phase systems comprising solid particles evenly dispersed in a liquid. The size of these particles is a crucial parameter as it determines the very existence of sols, controls their thermodynamic stability, and avoids sedimentation by ensuring the dominance of thermal forces over gravitational forces. The International Union of Pure and Applied Chemistry suggests that the dispersed particles should have at least in one direction a dimension roughly between 1 nm and 1 μm or that in a system discontinuities are found at distances of that order [1]. This definition allows one to distinguish colloids from solutions, where solute and solvent are molecular species, and from suspensions, which incorporate particles that are much larger than 1 μm and eventually settle out. This property allows colloids to fill a niche that requires such properties, such as paints or shampoos. Nevertheless, in the literature it is not rare to find a very wide and perhaps confusing spectrum of supposedly identical definitions, including colloidal solutions and colloidal suspensions. In addition, there is a confounding use of the term *colloid* to refer to particles, rather than to the system in which these are dispersed. In what follows we employ the term *colloid* (or colloidal sol) to refer to a system of nanoparticles evenly dispersed in a liquid.

Nanoparticles immersed in liquids exhibit ceaseless random moves, which were first reported by the botanist Brown, who, almost two centuries ago, investigated the dynamics of pollen grains in water [2]. Due to the later theoretical works by Einstein [3], Sutherland [4], von Smoluchowski [5], and Langevin [6] and the experiments by Perrin and Hammick [7,8], we now know that such erratic movements, commonly

referred to as Brownian motion, stem from the thermal energy dissipated by the collision between colloidal particles and the molecules of the dispersing medium. According to these works, the mean-square displacement (MSD), which measures the ability of particles to displace a distance Δr with respect to a reference location, grows linearly in time, whereas the particle displacements follow a Gaussian distribution with zero mean. In particular, the MSD in three dimensions reads

$$\langle r^2 \rangle = 6Dt, \quad (1)$$

where D is the particle long-time diffusion coefficient in the fluid and t is the time. The linearity of the MSD with t is usually referred to as Fickian diffusion and is normally observed in most colloidal systems. Nevertheless, anomalous diffusive behaviors, where $\Delta r^2 \propto t^\gamma$ and γ is either lower (subdiffusion) or larger (superdiffusion) than 1, have been identified [9–15] and can be accompanied by Gaussian or non-Gaussian distributions of particle displacements. One might expect the occurrence of Gaussian deviations only in colloids displaying anomalous diffusion as the central limit theorem applied to random walks, which predicts Gaussianity and Fickianity at sufficiently long timescales, indeed supports this view [16]. However, there exist systems, whose dynamics is Fickian, but the distribution of their particle displacement is non-Gaussian, such as biological systems [17–20], supercooled liquids [21–23], colloidal systems [24–27], two-dimensional fluids [28–33], and fluids in porous media [34,35]. While this Fickian yet non-Gaussian (FNG) behavior is being increasingly identified in soft materials and its origin is the topic of an intense research debate [36–41], recent Brownian dynamics and dynamic Monte Carlo simulations of colloidal liquid crystals suggest that FNG dynamics might not be ubiquitous in soft matter [42,43].

In this work we employ Molecular Dynamics (MD) simulations to mimic the equilibrium dynamics of dense colloidal

*apatti@ugr.es

sols of triangular nanotrimers, made of three tangent spheres interacting via different potentials of the Mie family. Our goal is to explore their long-time diffusion and identify the key elements determining the system's structural relaxation at long times. Investigating such Mie-like nanotrimers has been motivated by a few considerations. First of all, the Mie potential, which offers the option of independently tuning repulsive and attractive energy terms, guarantees better accuracy in the analysis of the phase behavior compared to the more popular Lennard-Jones (LJ) potential. This flexibility allows one to better reproduce the tendencies observed experimentally in specific systems of interest. Second, nanotrimers are anisotropic particles without axial symmetry that are expected to exhibit a very rich self-assembly behavior, where positional and orientational ordering have the potential to generate very intriguing crystal phases. We have so far only explored the stability domain of the low-density and high-density isotropic phases, as this knowledge is instrumental to examining the dynamics, and we are currently investigating the formation of ordered nanostructures. The kinetics of formation of these nanostructures would depend on the diffusion of the high-density isotropic phase of the nanotrimers; thus knowing the diffusive properties of the nanotrimers allows for further research into the structures formed. Finally, the complex geometry of nanotrimers, coupled to the possibility of tuning the degree of hardness of their interactions, provides an excellent model system to study the equilibrium dynamics over time and ponder the occurrence of FNG behavior at sufficiently long times, when a full structural relaxation decay is expected.

This paper is organized as follows. In Sec. II we discuss the particle model and the simulation methods employed to investigate equilibrium and dynamics of isotropic sols of nanotrimers. Since MD simulation is a standard technique, we will only highlight those elements that are instrumental for the interested reader to reproduce our results. In this section we also introduce the main dynamical properties that have been estimated to characterize the behavior of our systems. In Sec. III we first report on the phase behavior of colloidal nanotrimers as a function of the hardness of the Mie potential explored here. Then we focus on the long-time dynamics by assessing the ability of nanotrimers to diffuse and the existence of slow and fast particles that together determine the system's structural relaxation decay. In Sec. IV we summarize and provide conclusions.

II. METHODS

We performed MD simulations of rigid nanotrimers made of three identical spherical beads of diameter σ , the system unit length. The solvent is not explicitly modeled, but included in the effective interactions established between particles. We stress that implicit-solvent MD simulations create ballistic trajectories at very short times, when stochastic trajectories are rather expected. This artificial scenario extends only up to the so-called cage regime, when each particle starts to interact with its neighbors, and does not affect the long-time dynamics, which is governed by particle-particle collisions [44–46]. The beads comprising a nanotrimer are tangential to one another and at a mutual distance given by σ , as schematically shown in the inset of Fig. 1. The interactions established

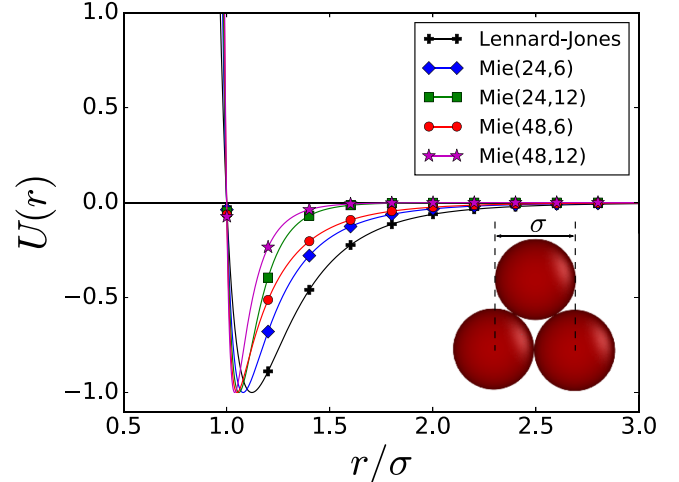


FIG. 1. Mie potentials employed in this study as a function of the distance between the center of mass of nonbonded beads and their comparison with the LJ potential. The inset shows the tangent-sphere model used to mimic a nanotrimer.

between nonbonded beads, namely, by beads belonging to distinct nanotrimers, are described by the Mie potential, which reads [47]

$$U(r) = C\epsilon \left[\left(\frac{\sigma}{r} \right)^n - \left(\frac{\sigma}{r} \right)^m \right], \quad (2)$$

where ϵ is the depth of the potential well, whereas the exponents n and m set the range of repulsive and attractive contributions, respectively. The coefficient C in Eq. (2) is given by

$$C \equiv \left(\frac{n}{n-m} \right) \left(\frac{n}{m} \right)^{m/(n-m)} \quad (3)$$

and is defined such that the minimum of the potential is $-\epsilon$. In this work the potential is cut and shifted at the cutoff distance of $r_c = 3\sigma$ to allow the whole nanotrimer to interact with its nearest neighbors. The Mie potential is a more flexible version of the standard LJ potential, which can be recovered by setting $n = 12$ and $m = 6$. By separately modifying m and n , one can *de facto* fine-tune the chemistry of the nanotrimers and ultimately the effective interactions between them and the implicit dispersing solvent. For instance, by increasing the attractive or repulsive exponents in Eq. (2), the critical temperature of the fluid-fluid phase coexistence decreases and, in the limit of very large values of attractive or repulsive exponents, this coexistence becomes metastable and embedded within the fluid-solid coexistence. The specific (n, m) pairs explored in this work are (24,6), (24,12), (48,6), and (48,12) and the resulting potentials will be referred to as $\text{Mie}(n, m)$ in the following. The functional form of these four potentials is reported in Fig. 1 and compared to the standard LJ or $\text{Mie}(12, 6)$ potential.

All simulations were performed using the Large-scale Atomic/Molecular Massively Parallel Simulator (LAMMPS) package [48]. To determine the fluid-fluid phase coexistence of each Mie potential, we arranged $N = 2458$ nanotrimers in elongated orthogonal boxes of sides $L_x = L_y = 16\sigma$, and $L_z = 80\sigma$ with periodic boundary conditions at different

reduced temperatures. In particular, the reduced temperature is defined as $T^* \equiv k_B T / \epsilon$, with T the absolute temperature and k_B the Boltzmann constant, whereas the reduced density is $\rho^* \equiv \rho \sigma^3$, where ρ is the number density of the nanotrimers in the system. At equilibrium, systems phase separated into a low-density isotropic phase and a high-density isotropic phase, the densities of which may be obtained. The critical properties of each system were determined using the expressions [49]

$$\rho_{\text{HD}} - \rho_{\text{LD}} = C_1(T_c - T)^{\beta_c}, \quad (4)$$

$$\frac{\rho_{\text{HD}} + \rho_{\text{LD}}}{2} = \rho_c - C_2(T_c - T), \quad (5)$$

where T_c is the critical temperature, ρ_c is the critical density, ρ_{LD} and ρ_{HD} are the densities of the low-density and high-density fluid phases, respectively, $\beta_c = 0.325$ is the critical exponent obtained from renormalization-group theory, and C_1 and C_2 are fitting parameters. Locating T_c and ρ_c was especially important to consistently compare the dynamics of the four different sets of Mie potentials.

To study the dynamics, we then selected high-density fluid states in the one-phase region of existence of high-density fluids. In this case, we arranged $N = 2000$ nanotrimers in cubic boxes of varying sizes, depending on the required density, with periodic boundary conditions and equilibrated them in the canonical (NVT) ensemble. More specifically, equilibration runs took approximately 2×10^5 time steps, with an elementary time step set to $t = 10^{-4}\tau$, where $\tau = \sqrt{M\sigma^2/\epsilon}$ is the system time unit and M the mass of one nanotrimer bead. Systems were considered at equilibrium when their total energy achieved a steady-state value within statistical fluctuations. Subsequently, 300 independent time trajectories, each consisting of 4×10^6 time steps, were used to calculate the dynamical properties of interest. To keep the temperature constant, we applied the Nosé-Hoover thermostat.

To compare the behavior of systems exhibiting different phase diagrams, we opted to assess structural and dynamical properties at the same reduced temperature and density, defined as $T_r \equiv T/T_c$ and $\rho_r \equiv \rho_{\text{HD}}/\rho_c$, respectively. At $T_r = 0.95$ and $\rho_r = 2.5$, all systems are dense fluids with no evidence of crystallization, which is expected to be observed at larger densities, and furthermore, the high temperature of the fluids ensures that the systems do not get arrested or enter glasslike dynamical regimes. Therefore, the selected values of reduced temperature and density are indeed suitable to coherently compare structure and dynamics of the systems studied here. We have also explored other state points for these systems and found no relevant differences in the dynamics, apart from the expected variations due to changes in temperature and density in the high-density fluid phase. The specific sets of temperature and density of the high-density fluid phases for each Mie potential are reported in Table I.

To investigate the long-time relaxation dynamics of nanotrimers in dense fluids, we calculated a number of dynamical properties. More specifically, the MSD, which can be used to determine the self-diffusion coefficients, reads

$$\langle r^2(t) \rangle = \frac{1}{N} \left\langle \sum_{j=1}^N [\mathbf{r}_j(t) - \mathbf{r}_j(0)]^2 \right\rangle, \quad (6)$$

TABLE I. State points used in the simulations for each potential to study dynamical properties.

$U(r)$	T^*	ρ_{HD}^*	T_c^*	ρ_c^*	T_r	ρ_r
Mie(24,6)	1.270	0.253	1.337	0.101	0.95	2.5
Mie(48,6)	1.027	0.263	1.081	0.105	0.95	2.5
Mie(24,12)	0.725	0.290	0.764	0.116	0.95	2.5
Mie(48,12)	0.577	0.315	0.607	0.126	0.95	2.5

where $\langle \dots \rangle$ indicates ensemble average and $\mathbf{r}_j(t)$ indicates the location of the center of mass of nanotrimer j at time t . The distribution of displacements over time and hence the occurrence of fast and slow nanotrimers was investigated by computing the self part of the Van Hove correlation function given by

$$G_s(r, t) = \frac{1}{N} \left\langle \sum_{j=1}^N \delta(r - |\mathbf{r}_j(t) - \mathbf{r}_j(0)|) \right\rangle, \quad (7)$$

where δ is the Dirac delta function. The $G_s(r, t)$ was normalized such that $\int_0^\infty 4\pi r^2 G_s dr = 1$ [42]. Deviations from Gaussian dynamics were assessed by using the non-Gaussian parameter α_2 defined as

$$\alpha_2(t) = \frac{\langle \Delta r^4(t) \rangle}{(1 + 2/d) \langle \Delta r^2(t) \rangle^2} - 1, \quad (8)$$

where d is the dimensionality of the system studied. The non-Gaussian parameter is obtained from the first term of the Hermite polynomial expansion of the $G_s(r, t)$ [50]. Finally, to provide a quantitative measure of the time needed to observe the structural relaxation of the systems and to quantify the decay of their density fluctuations, we calculate the self-intermediate scattering function (SISF), which reads

$$F_s(\mathbf{q}, t) = \frac{1}{N} \left\langle \sum_{j=1}^N \exp[i\mathbf{q} \cdot (\mathbf{r}_j(t) - \mathbf{r}_j(0))] \right\rangle, \quad (9)$$

where \mathbf{q} is the wave vector defined at the main peak of the static structure factor [27].

III. RESULTS

Before discussing the details of the long-time relaxation dynamics of our colloidal nanotrimers, we first report on their phase behavior, limiting our attention to the fluid phases. In particular, the temperature vs density phase diagrams of nanotrimers interacting via the potentials Mie(24,6), Mie(48,6), Mie(24,12), and Mie(48,12) are presented in Fig. 2.

The coexistence between the low-density and high-density fluid phases has been investigated in elongated boxes of the type shown in the inset of the same figure. Following equilibration, the density of each phase was estimated by calculating the number of nanotrimers in volume elements $L_x \hat{\mathbf{x}} \cdot L_y \hat{\mathbf{y}} \cdot \delta_z \hat{\mathbf{z}}$, with $\delta_z = L_z/500$, located far enough from the interface, where fluctuations are larger, and averaged over multiple uncorrelated configurations to reduce statistical noise. The calculated fluid phase coexistence diagrams are shown in Fig. 2. One can observe that critical temperature and critical density have an opposite dependence on the nature

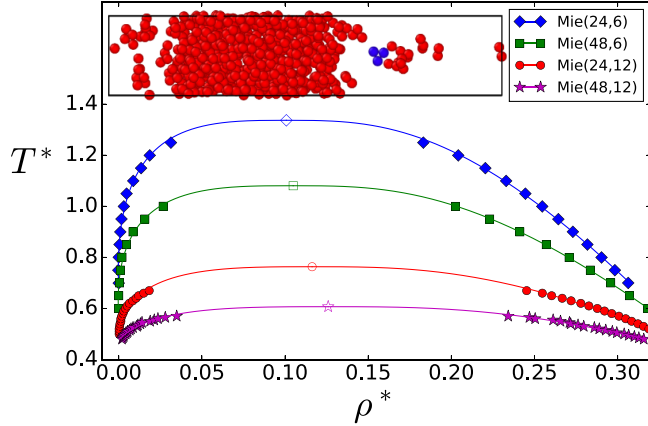


FIG. 2. Fluid-fluid phase coexistence diagrams of colloidal suspensions comprised of nanotrimers interacting via the Mie potentials listed in the legend. Closed symbols are simulation results, open symbols are the critical points estimated using Eqs. (4) and (5), and solid lines are guides for the eye. The inset shows a typical equilibrium configuration with one nanotrimer highlighted in blue.

of the Mie potential as the former monotonically decreases from Mie(24,6) to Mie(48,12), whereas the latter increases. These tendencies agree well with findings that highlighted the dependence of the critical point on the potential hardness [51]. In particular, the potential hardness can be estimated by computing the parameter

$$H(n, m) = \mathcal{C} \left[\left(\frac{1}{m-3} \right) - \left(\frac{1}{n-3} \right) \right], \quad (10)$$

which has been obtained from the mean-field approximation of the first-order term of the Barker-Henderson perturbation theory [51]. The values of H for each potential are indicated in Table II, with lower values of H indicating harder potentials. The table, in conjunction with Table I, shows a clear correlation of the decrease in H to the decreases in critical temperature and increases in critical density in the systems of nanotrimers.

Identifying the binodal line was a preliminary step to locate the region where the high-density fluid, whose dynamical properties we wanted to investigate, is stable. To ensure that these properties would not be calculated in the crystal phases that are expected to form at sufficiently large densities, we double-checked the fluid structure by calculating the radial distribution function $g(r)$ of the nanotrimers' centers of mass. These distribution functions, which are reported in Fig. 3 for each of the four state points listed in Table I, exhibit a primary

TABLE II. Self-diffusion coefficient D^* evaluated at $T_r = 0.95$ and $\rho_r = 2.5$ for different Mie potentials. Their corresponding hardness H is also presented.

$U(r)$	H	D^*
Mie(24,6)	0.605	0.0496
Mie(48,6)	0.479	0.0340
Mie(24,12)	0.254	0.0130
Mie(48,12)	0.188	0.0052

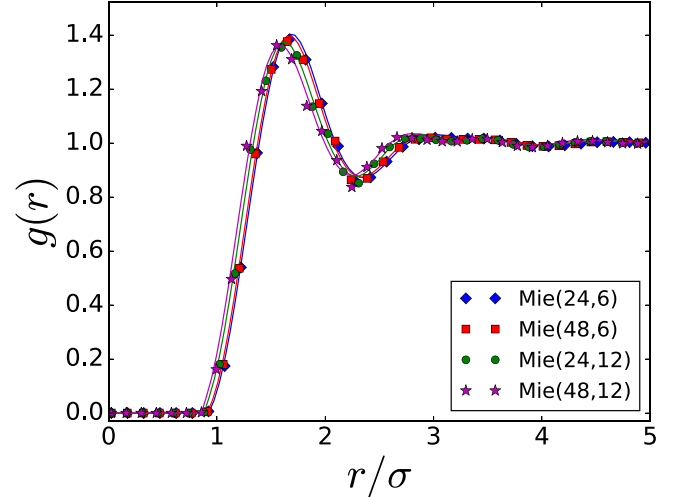


FIG. 3. Radial distribution functions of nanotrimers' center of mass at $\rho_r = 2.5$ and $T_r = 0.95$ for the four Mie potentials reported in the legend. The symbols show simulation data and the lines are guides for the eye.

peak at approximately $r/\sigma = 1.5$ and then converge to unity at the typically short distances detected in liquidlike systems. Having established that these are indeed fluid phases, we can now discuss the main features of their long-time relaxation dynamics.

To this end, we first estimated the MSD of nanotrimers, which is reported in Fig. 4(a). It can be observed that different interaction potentials are not significantly affecting the MSD, especially so at short timescales, when the system is still in the ballistic regime and $\langle r^2 \rangle \propto t^2$. It should be noticed that implicit-solvent MD simulations cannot reproduce the Brownian motion of colloids at short timescales, where a diffusive regime is expected [45,46]. The fully deterministic nature of MD produces an artificial ballistic regime at very short times, when particles are still displacing within the cage formed by their neighbors. Nevertheless, as soon as the particle-particle collisions become the dominant element controlling the system's dynamics, these effects become less and less relevant and eventually fade at sufficiently long times, where the MSDs as obtained from MD and Brownian dynamics simulations collapse onto each other [45,46]. In our specific case, the four systems studied enter the long-time diffusive regime at approximately $1 < t/\tau < 10$ and, from this time on, $\langle r^2 \rangle \propto t$ as expected in Brownian systems.

The onset of the linearity of the MSD with time, also referred to as Fickian diffusion, can be more accurately located by calculating the dependence of the exponent γ of the power law $\langle r^2 \rangle \propto t^\gamma$ over time. We know that for $\gamma = 2$ the dynamics is ballistic, whereas for $\gamma = 1$ the dynamics is diffusive. In particular, $\gamma = d \ln \langle r^2 \rangle / d \ln t$ is reported in Fig. 4(b) and exhibits a relatively fast decay to 1, confirming the beginning of the long-time diffusive regime at approximately $t^* = t/\tau = 1$, depending on the Mie potential. It is interesting to observe that Mie(24,12) and Mie(48,12) nanotrimers experience a slightly subdiffusive dynamics between $t/\tau = 1$ and 10^2 , with $0.9 < \gamma < 1$. It is an almost negligible effect as γ is still rather large, but it is anyway not observed

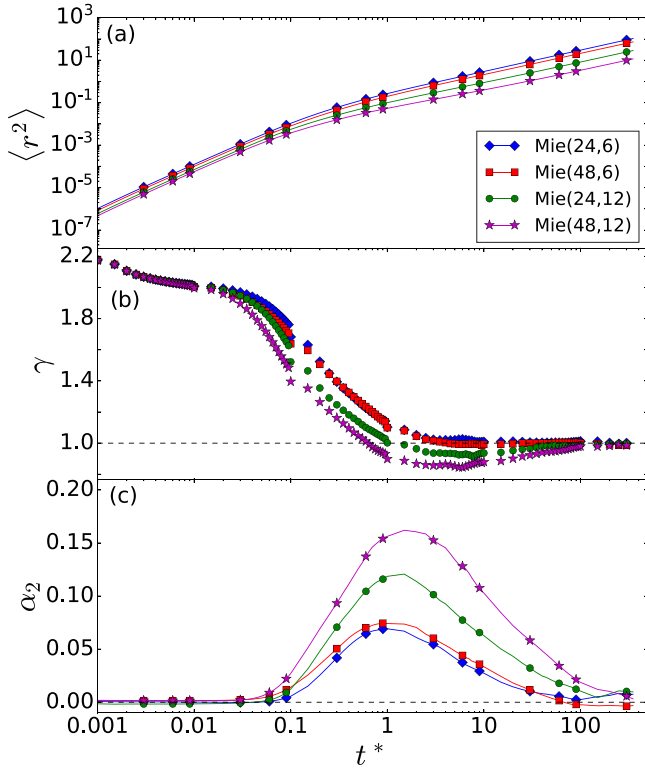


FIG. 4. (a) MSD as a function of time for the systems interacting via the Mie potentials reported in the legend. The state points of the systems correspond to a temperature of $T_r = 0.95$ and a density of $\rho_r = 2.5$. (b) Log-derivative of the MSD, which corresponds to the slope of the MSDs presented in (a). The dashed line corresponds to the value of $\gamma = 1$, which indicates the onset of Fickian diffusion. (c) Non-Gaussian parameter as a function of time. The dashed line at $\alpha_2 = 0$ indicates when the systems exhibit Gaussian dynamics.

with Mie(24,6) and Mie(48,6) nanotrimers, whose exponent γ never falls below 1. We believe that this is most likely due to the particle-particle attractive interactions being dominant over the kinetic energy of the particles at the temperatures of the simulations for $n = 12$ compared to $n = 6$ and thus slowing particles down when these are just about to diffuse through the cage of neighbors. The cage effect itself is expected to be stronger for more attractive nanotrimers, but this is not especially evident from the analysis of the MSD as the crossover from the ballistic to the diffusive regime appears to be equally smooth for the four Mie potentials. Fickian diffusion allows for the calculation of the self-diffusion coefficient of the different nanotrimer systems using Eq. (1). The coefficients are reported in Table II and follow the pattern shown by the hardness of the potentials, with the harder potentials diffusing slower. This decrease in diffusivity is most likely caused by the differences in particle-particle interaction strength between the potentials, as stronger particle-particle interactions will impede the ability of nanotrimers to diffuse through the system.

Changing the form of the Mie potential has also a relevant effect on the time associated with the structural relaxation of the system, which has been measured by computing the SISFs, reported in Fig. 5. This time, referred to as the α -relaxation

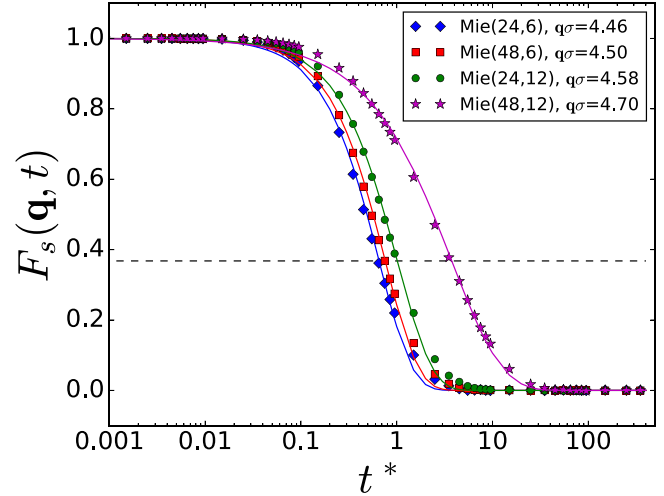


FIG. 5. Self-intermediate scattering functions of the four systems studied. Symbols are simulation results, while solid lines are exponential fits of the type $\exp[(-t/t_\alpha)^a]$, with t_α and a fitting parameters. The dashed line represents the value $F_s = 1/e$, at which structural relaxation is considered achieved and defines the α -relaxation time for each potential.

time, is achieved when $F_s(\mathbf{q}, t) = 1/e$. Much denser systems, such as glasses and subcooled liquids, can also show a β -relaxation time, corresponding to the short-time relaxation at the particle scale, occurring over the so-called cage regime. Our systems, which are not as dense, are characterized by a single structural relaxation decay. In particular, t_α/τ ranges between 0.6 for Mie(24,6) and 3.7 for Mie(48,12), as shown in Table III. While quantitatively different, the four SISFs show a very similar qualitative behavior, characterized by an exponential decay of the type $\exp[(-t/t_\alpha)^a]$, with t_α and $a \approx 1$ fitting parameters.

Deviations from Gaussian dynamics have been investigated by analyzing the non-Gaussian parameter α_2 defined in Eq. (8) and reported in Fig. 4(c). As a general tendency, we notice that deviations are relatively small compared to other soft-matter systems, such as colloidal glasses, crystals, and liquid crystals, where α_2 was found to be more than one order of magnitude larger [52–58]. All systems exhibit a Gaussian dynamics at short timescales with $\alpha_2 = 0$ up to $t/\tau \approx 0.1$, although deviations are already noticeable for the Mie(48,12) potential. At intermediate times, α_2 increases and reaches its maximum at $1 < t/\tau < 2$, corresponding to the onset of the diffusive regime. We notice that the peak amplitude increases with the potential hardness, suggesting that particle-particle attractions dominate over repulsive forces in determining the extent of deviations from Gaussian behavior.

TABLE III. Values of α -relaxation time for different Mie potentials.

$U(r)$	$q\sigma$	t_α/τ
Mie(24,6)	4.46	0.65
Mie(48,6)	4.50	0.76
Mie(24,12)	4.58	1.01
Mie(48,12)	4.70	3.75

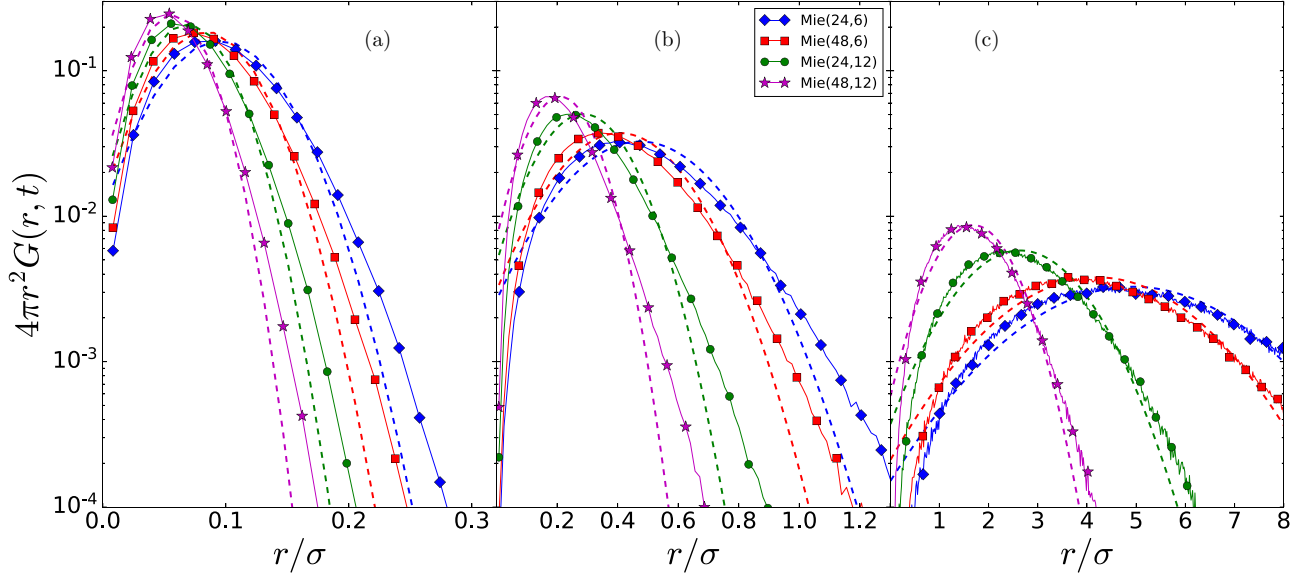


FIG. 6. Self part of the Van Hove correlation functions at (a) $t^* = 0.1$, (b) $t^* = 1$, and (c) $t^* = 100$ in systems of nanotrimers interacting via the Mie potentials shown in the legend. Symbols represent simulation results, solid lines are guides for the eye, and dashed lines are Gaussian approximations.

This result is in line with the above-mentioned subdiffusive dynamics observed in Mie(48,12) systems over the same time window where α_2 is larger than zero. In particular, the temporary non-Gaussian dynamics of especially attractive nanotrimers is accompanied by an equally temporary non-Fickianity that is completely negligible in systems interacting through the Mie(24,6) and Mie(48,6) potentials. At sufficiently long times, namely, for $t/\tau \geq 100$, all systems recover a full Gaussian and Fickian dynamics, with $\alpha_2 \approx 0$ and $\gamma \approx 1$. The relatively modest magnitude of the non-Gaussian parameter suggests that the nanotrimers' dynamics is essentially Gaussian at short and long times and slightly non-Gaussian at intermediate times. In particular, at long timescales the dynamics is Fickian ($\langle r^2 \rangle \propto t$) and Gaussian ($\alpha = 0$), confirming that FNG dynamics is not necessarily a distinctive feature of soft materials, as recently observed in nematic liquid crystals of uniaxial [42,59,60] and biaxial [61] particles.

The temporary deviations from Gaussianity can also be detected by the analysis of the self part of the Van Hove correlation functions, which are reported in Fig. 6 at short ($t/\tau = 0.1$), intermediate ($t/\tau = 1$), and long ($t/\tau = 100$) times. These functions offer insight into the probability distribution of particle displacements and are especially convenient to ponder the existence of slow and fast particles that, respectively, displace distances that are much shorter or longer than the average. For each curve, we include the Gaussian fits (dashed lines) that quantify deviations from a normal distribution of displacements. The Gaussian fits are generally very good at short and long times, with an R^2 between 0.95 and 0.99 across the three timescales reported in Fig. 6. A more accurate analysis shows that these fits overestimate the probability of short displacements and underestimate that of long displacements. In other words, at short, intermediate, and long timescales, the probability of observing slow and fast particles is, respectively, lower and higher than what a

Gaussian distribution of displacements would predict. This is especially evident for systems of Mie(24,12) and Mie(48,12) nanotrimers, which, due to the stronger particle-particle attractions, are less mobile and thus less likely to displace much longer distances than the average. By contrast, Mie(24,6) and Mie(48,6) particles are significantly more mobile and hence more likely to displace relatively long distances as the tail of the self part of the Van Hove functions in Fig. 6 shows.

IV. CONCLUSION

In summary, by MD simulations we have investigated the long-time relaxation dynamics of colloidal nanotrimers that interact via a range of Mie potentials. Tuning the strength of repulsive and attractive particle-particle interactions sets the potential hardness, which in turns determines the system phase behavior and dynamics. The former was investigated by calculating the region of coexistence between the low-density and high-density fluid phases and the corresponding critical point. Determining the location of the critical point was crucial to set the reduced temperature and density at which all systems existed as dense fluids and thus consistently compare their dynamical properties. To this end, we calculated the mean-square displacements and their derivative with respect to time and found that a full long-time diffusive regime is achieved at approximately $t/\tau \approx 1$, when most nanotrimers have displaced a distance between 0.1σ and 0.5σ . In addition, $t/\tau \approx 1$ is also the time the SISF shows the systems undergo α relaxation and the non-Gaussian parameter, which quantifies the deviations from Gaussian dynamics, reaches its maximum value and then decays to zero at longer times. In general, these deviations are not significant, with the R^2 of the self part of the Van Hove function never having a value below 0.95. While the deviations are small, especially if compared to those detected in colloidal liquid crystals, crystals, and glasses [52–58], they help one appreciate the impact of attractive

interactions on nanotrimers' dynamics and on the onset of the diffusive regime. In particular, the Mie(48,12) potential shows a slight subdiffusive behavior, with $0.9 < \gamma < 1$, that extends over at least two time decades and is not observed in systems of Mie(48,6) nanotrimers, which are significantly more repulsive and exhibit a more pronounced mobility. The computation of the self part of the Van Hove correlation functions reveals the essentially Gaussian nature of distribution of displacements and indicates that deviations from Gaussianity are observed at short, intermediate, and long times, but become less and less relevant as soon as the diffusive regime fully develops. The self part of the Van Hove functions also highlight the occurrence of slow and fast nanotrimers that are mostly observed in Mie(48,12) and Mie(24,6) systems, respectively. The former comprise particles whose attractive interactions are especially strong and are thus more prone to stick together and consequently less mobile. By contrast, weaker attractive interactions enhance the mobility of

particles, which end up displacing significantly longer distances than the average. Finally, the simultaneous occurrence of Gaussianity and Fickianity at long times unambiguously confirms the Brownian nature of the Mie nanotrimers' dynamics and reinforces the idea that FNG dynamics is not a universal signature of soft-matter systems.

ACKNOWLEDGMENTS

This work was supported by the UK Engineering and Physical Sciences Research Council via an Industrial Cooperative Award in Science and Technology cofunded by IBM. A.P. is supported by a Maria Zambrano Senior distinguished researcher fellowship, financed by the European Union within the NextGenerationEU program. The authors would like to acknowledge the assistance given by Research IT and the use of the Computational Shared Facility at The University of Manchester.

-
- [1] A. D. McNaught and A. Wilkinson, *Compendium of Chemical Terminology*, 2nd ed. (Blackwell, Oxford, 1997).
- [2] R. Brown, in *The Miscellaneous Botanical Works of Robert Brown*, edited by J. J. Bennett (Cambridge University Press, Cambridge, 2015), Vol. 1, pp. 463–486.
- [3] A. Einstein, On the movement of small particles suspended in stationary liquids required by the molecular-kinetic theory of heat, *Ann. Phys. (Leipzig)* **322**, 549 (1905).
- [4] W. Sutherland, LXXV. A dynamical theory of diffusion for non-electrolytes and the molecular mass of albumin, *Philos. Mag.* **9**, 781 (1905).
- [5] M. von Smoluchowski, Zur kinetischen theorie der Brownschen molekularbewegung und der suspensionen, *Ann. Phys. (Leipzig)* **326**, 756 (1906).
- [6] P. Langevin, Sur la théorie du mouvement Brownien, *C. R. Acad. Sci. (Paris)* **146**, 530 (1908).
- [7] J. Perrin, Mouvement Brownien et réalité moléculaire, *Ann. Chim. Phys.* **18**, 5 (1909).
- [8] J. Perrin and D. Hammick, *Atoms* (Van Nostrand, New York, 1916).
- [9] J.-P. Bouchaud and A. Georges, Anomalous diffusion in disordered media: Statistical mechanisms, models and physical applications, *Phys. Rep.* **195**, 127 (1990).
- [10] I. Golding and E. C. Cox, Physical Nature of Bacterial Cytoplasm, *Phys. Rev. Lett.* **96**, 098102 (2006).
- [11] A. V. Weigel, B. Simon, M. M. Tamkun, and D. Krapf, Ergodic and nonergodic processes coexist in the plasma membrane as observed by single-molecule tracking, *Proc. Natl. Acad. Sci. U.S.A.* **108**, 6438 (2011).
- [12] R. Metzler, J.-H. Jeon, A. G. Cherstvy, and E. Barkai, Anomalous diffusion models and their properties: Non-stationarity, non-ergodicity, and ageing at the centenary of single particle tracking, *Phys. Chem. Chem. Phys.* **16**, 24128 (2014).
- [13] J.-H. Jeon, M. Javanainen, H. Martinez-Seara, R. Metzler, and I. Vattulainen, Protein Crowding in Lipid Bilayers Gives Rise to Non-Gaussian Anomalous Lateral Diffusion of Phospholipids and Proteins, *Phys. Rev. X* **6**, 021006 (2016).
- [14] W. Wang, A. G. Cherstvy, X. Liu, and R. Metzler, Anomalous diffusion and nonergodicity for heterogeneous diffusion processes with fractional Gaussian noise, *Phys. Rev. E* **102**, 012146 (2020).
- [15] A. G. Cherstvy, H. Safdari, and R. Metzler, Anomalous diffusion, nonergodicity, and ageing for exponentially and logarithmically time-dependent diffusivity: Striking differences for massive versus massless particles, *J. Phys. D* **54**, 195401 (2021).
- [16] C. Tsallis, S. V. F. Levy, A. M. C. Souza, and R. Maynard, Statistical-Mechanical Foundation of the Ubiquity of Lévy Distributions in Nature, *Phys. Rev. Lett.* **75**, 3589 (1995).
- [17] T. Toyota, D. A. Head, C. F. Schmidt, and D. Mizuno, Non-Gaussian athermal fluctuations in active gels, *Soft Matter* **7**, 3234 (2011).
- [18] K. C. Leptos, J. S. Guasto, J. P. Gollub, A. I. Pesci, and R. E. Goldstein, Dynamics of Enhanced Tracer Diffusion in Suspensions of Swimming Eukaryotic Microorganisms, *Phys. Rev. Lett.* **103**, 198103 (2009).
- [19] B. R. Parry, I. V. Surovtsev, M. T. Cabeen, C. S. O'Hern, E. R. Dufresne, and C. Jacobs-Wagner, The bacterial cytoplasm has glass-like properties and is fluidized by metabolic activity, *Cell* **156**, 183 (2014).
- [20] S. Hapca, J. W. Crawford, and I. M. Young, Anomalous diffusion of heterogeneous populations characterized by normal diffusion at the individual level, *J. R. Soc. Interface.* **6**, 111 (2009).
- [21] G. Szamel and E. Flenner, Time scale for the onset of Fickian diffusion in supercooled liquids, *Phys. Rev. E* **73**, 011504 (2006).
- [22] W. Kob, C. Donati, S. J. Plimpton, P. H. Poole, and S. C. Glotzer, Dynamical Heterogeneities in a Supercooled Lennard-Jones Liquid, *Phys. Rev. Lett.* **79**, 2827 (1997).
- [23] R. Das, C. Dasgupta, and S. Karmakar, Time scales of Fickian diffusion and the lifetime of dynamic heterogeneity, *Front. Phys.* **8**, 210 (2020).

- [24] I. Chakraborty and Y. Roichman, Disorder-induced Fickian, yet non-Gaussian diffusion in heterogeneous media, *Phys. Rev. Research* **2**, 022020(R) (2020).
- [25] B. Wang, S. M. Anthony, C. B. Sung, and S. Granick, Anomalous yet Brownian, *Proc. Natl. Acad. Sci. U.S.A.* **106**, 15160 (2009).
- [26] C. Xue, X. Zheng, K. Chen, Y. Tian, and G. Hu, Probing non-Gaussianity in confined diffusion of nanoparticles, *J. Phys. Chem. Lett.* **7**, 514 (2016).
- [27] A. L. Thorneywork, D. G. A. L. Aarts, J. Horbach, and R. P. A. Dullens, On the Gaussian approximation in colloidal hard sphere fluids, *Soft Matter* **12**, 4129 (2016).
- [28] W. Chen and K. To, Unusual diffusion in a quasi-two-dimensional granular gas, *Phys. Rev. E* **80**, 061305 (2009).
- [29] Z. Ghannad, Fickian yet non-Gaussian diffusion in two-dimensional Yukawa liquids, *Phys. Rev. E* **100**, 033211 (2019).
- [30] R. Pastore, A. Ciarlo, G. Pesce, F. Greco, and A. Sasso, Rapid Fickian Yet Non-Gaussian Diffusion after Subdiffusion, *Phys. Rev. Lett.* **126**, 158003 (2021).
- [31] S. K. Schnyder, T. O. E. Skinner, A. L. Thorneywork, D. G. A. L. Aarts, J. Horbach, and R. P. A. Dullens, Dynamic heterogeneities and non-Gaussian behavior in two-dimensional randomly confined colloidal fluids, *Phys. Rev. E* **95**, 032602 (2017).
- [32] G. Kwon, B. J. Sung, and A. Yethiraj, Dynamics in crowded environments: Is non-Gaussian Brownian diffusion normal? *J. Phys. Chem. B* **118**, 8128 (2014).
- [33] J. Kim, C. Kim, and B. J. Sung, Simulation Study of Seemingly Fickian but Heterogeneous Dynamics of Two Dimensional Colloids, *Phys. Rev. Lett.* **110**, 047801 (2013).
- [34] K. He, F. B. Khorasani, S. T. Retterer, D. K. Thomas, J. C. Conrad, and R. Krishnamoorti, Diffusive dynamics of nanoparticles in arrays of nanoposts, *ACS Nano* **7**, 5122 (2013).
- [35] K. He, S. T. Retterer, B. R. Srijanto, J. C. Conrad, and R. Krishnamoorti, Transport and dispersion of nanoparticles in periodic nanopost arrays, *ACS Nano* **8**, 4221 (2014).
- [36] B. Wang, J. Kuo, S. C. Bae, and S. Granick, When Brownian diffusion is not Gaussian, *Nat. Mater.* **11**, 481 (2012).
- [37] M. V. Chubynsky and G. W. Slater, Diffusing Diffusivity: A Model for Anomalous, yet Brownian, Diffusion, *Phys. Rev. Lett.* **113**, 098302 (2014).
- [38] A. V. Chechkin, F. Seno, R. Metzler, and I. M. Sokolov, Brownian yet Non-Gaussian Diffusion: From Superstatistics to Subordination of Diffusing Diffusivities, *Phys. Rev. X* **7**, 021002 (2017).
- [39] M. Matse, M. V. Chubynsky, and J. Bechhoefer, Test of the diffusing-diffusivity mechanism using near-wall colloidal dynamics, *Phys. Rev. E* **96**, 042604 (2017).
- [40] V. Sposini, A. V. Chechkin, F. Seno, G. Pagnini, and R. Metzler, Random diffusivity from stochastic equations: Comparison of two models for Brownian yet non-Gaussian diffusion, *New J. Phys.* **20**, 043044 (2018).
- [41] J. M. Miotto, S. Pigolotti, A. V. Chechkin, and S. Roldán-Vargas, Length Scales in Brownian yet Non-Gaussian Dynamics, *Phys. Rev. X* **11**, 031002 (2021).
- [42] A. Cuetos, N. Morillo, and A. Patti, Fickian yet non-Gaussian diffusion is not ubiquitous in soft matter, *Phys. Rev. E* **98**, 042129 (2018).
- [43] L. Tonti, F. A. G. Daza, and A. Patti, Diffusion of globular macromolecules in liquid crystals of colloidal cuboids, *J. Mol. Liq.* **338**, 116640 (2021).
- [44] D. Frenkel and B. Smit, *Understanding Molecular Simulation*, 2nd ed. (Elsevier, Amsterdam, 2002).
- [45] L. López-Flores, L. L. Yeomans-Reyna, M. Chávez-Páez, and M. Medina-Noyola, The overdamped van Hove function of atomic liquids, *J. Phys.: Condens. Matter* **24**, 375107 (2012).
- [46] L. López-Flores, H. Ruíz-Estrada, M. Chávez-Páez, and M. Medina-Noyola, Dynamic equivalences in the hard-sphere dynamic universality class, *Phys. Rev. E* **88**, 042301 (2013).
- [47] G. Mie, Zur kinetischen theorie der einatomigen korper, *Ann. Phys. (Leipzig)* **316**, 657 (1903).
- [48] S. Plimpton, A. Thompson, S. Moore, A. Kohlmeyer, and R. Berger, LAMMPS molecular dynamics simulator.
- [49] D. A. Kofke, Direct evaluation of phase coexistence by molecular simulation via integration along the saturation line, *J. Chem. Phys.* **98**, 4149 (1993).
- [50] A. Rahman, Correlations in the motion of atoms in liquid argon, *Phys. Rev.* **136**, A405 (1964).
- [51] N. S. Ramrattan, C. Avendaño, E. A. Müller, and A. Galindo, A corresponding-states framework for the description of the Mie family of intermolecular potentials, *Mol. Phys.* **113**, 932 (2015).
- [52] A. Patti, D. El Masri, R. van Roij, and M. Dijkstra, Stringlike Clusters and Cooperative Interlayer Permeation in Smectic Liquid Crystals Formed by Colloidal Rods, *Phys. Rev. Lett.* **103**, 248304 (2009).
- [53] A. Patti, D. El Masri, R. van Roij, and M. Dijkstra, Collective diffusion of colloidal hard rods in smectic liquid crystals: Effect of particle anisotropy, *J. Chem. Phys.* **132**, 224907 (2010).
- [54] S. Belli, A. Patti, R. van Roij, and M. Dijkstra, Heterogeneous dynamics in columnar liquid crystals of parallel hard rods, *J. Chem. Phys.* **133**, 154514 (2010).
- [55] R. Matena, M. Dijkstra, and A. Patti, Non-Gaussian dynamics in smectic liquid crystals of parallel hard rods, *Phys. Rev. E* **81**, 021704 (2010).
- [56] Z. Zheng, F. Wang, and Y. Han, Glass Transitions in Quasi-Two-Dimensional Suspensions of Colloidal Ellipsoids, *Phys. Rev. Lett.* **107**, 065702 (2011).
- [57] A. Patti, S. Belli, R. van Roij, and M. Dijkstra, Relaxation dynamics in the columnar liquid crystal phase of hard platelets, *Soft Matter* **7**, 3533 (2011).
- [58] B. van der Meer, W. Qi, J. Sprakel, L. Filion, and M. Dijkstra, Dynamical heterogeneities and defects in two-dimensional soft colloidal crystals, *Soft Matter* **11**, 9385 (2015).
- [59] N. Morillo, A. Patti, and A. Cuetos, Brownian dynamics simulations of oblate and prolate colloidal particles in nematic liquid crystals, *J. Chem. Phys.* **150**, 204905 (2019).
- [60] D. Cywiak, A. Gil-Villegas, and A. Patti, Long-time relaxation dynamics in nematic and smectic liquid crystals of soft repulsive colloidal rods, *Phys. Rev. E* **105**, 014703 (2022).
- [61] A. Cuetos and A. Patti, Dynamics of hard colloidal cuboids in nematic liquid crystals, *Phys. Rev. E* **101**, 052702 (2020).